Molecular dynamics simulation of vibrational energy relaxation of highly excited molecules in fluids. III. Equilibrium simulations of vibrational energy relaxation of azulene in carbon dioxide

C. Heidelbach, V. S. Vikhrenko, D. Schwarzer, I. I. Fedchenia, and J. Schroeder

Citation: The Journal of Chemical Physics **111**, 8022 (1999); doi: 10.1063/1.480135
View online: http://dx.doi.org/10.1063/1.480135
View Table of Contents: http://scitation.aip.org/content/aip/journal/jcp/111/17?ver=pdfcov
Published by the AIP Publishing

Molecular dynamics simulation of vibrational energy relaxation of highly excited molecules in fluids. III. Equilibrium simulations of vibrational energy relaxation of azulene in carbon dioxide

C. Heidelbach, V. S. Vikhrenko,[a] D. Schwarzer, I. I. Fedchenia, and J. Schroeder[b]
Max-Planck-Institut für Biophysikalische Chemie, Am Fassberg 11, D-37077 Göttingen, Germany

(Received 25 February 1999; accepted 10 August 1999)

The expressions for vibrational energy relaxation (VER) rates of polyatomic molecules in terms of equilibrium capacity time correlation functions (TCFs) derived in the first paper of this series [J. Chem. Phys. **110**, 5273 (1999)] are used for the investigation of VER of azulene in carbon dioxide at low (3.2 MPa) and high (270 MPa) pressure. It is shown that for both cases the VER times evaluated on the basis of the same potential model via solute–solvent interaction capacity TCFs by means of equilibrium molecular dynamics (EMD) simulations satisfactorily agree with the nonequilibrium (NEMD) molecular dynamics [J. Chem. Phys. **110**, 5286 (1999)] and experimental [J. Chem. Phys. **105**, 3121 (1996)] results as well. Thus it follows that these methods can complement each other in characterizing VER from different points of view. Although more computational power and refined methods of dealing with simulated data are required for EMD simulations, they allow the use of powerful tools of equilibrium statistical mechanics for investigating the relaxation process. To this end, an analysis of VER mechanisms on the basis of normal mode and atomic representations is carried out. The influence of temperature and CO_2 pressure on azulene normal mode spectra and solvent assisted intermode coupling in connection with the eigenvector structure is investigated in great detail. The normal mode capacity cross-correlation matrix reveals the significance of intermode coupling, which significantly contributes to intramolecular vibrational energy redistribution (IVR). As a new concept, partial normal mode relaxation rates are introduced. It is shown that these rates demonstrate similar properties as the energy exchange rates through particular normal modes in nonequilibrium simulations. Atomic spectra and friction coefficients are characterized by a complicated frequency dependence due to contributions from many normal modes. Atomic capacity TCFs and partial relaxation rates are analyzed and reveal a similar picture to that obtained from NEMD simulations. These results show that VER and IVR cannot be separated from each other and have to be considered as mutually connected processes. © *1999 American Institute of Physics.* [S0021-9606(99)51641-3]

I. INTRODUCTION

Over the last years vibrational energy relaxation (VER) in liquids has been studied for a variety of systems both experimentally and theoretically[1–20] leading to an understanding of many factors affecting this type of process like oscillator frequency, solute–solvent interaction, mode of motions, temperature, and the significance of quantum mechanical aspects. But while most theoretical investigations have been dealing with small molecules consisting of only a few atoms, data are available[21–25] now for moderate size molecules, too.

VER of polyatomic molecules is a complex phenomenon comprising several distinct but mutually connected processes such as energy transfer from a vibrationally exited solute to the solvent, intramolecular energy redistribution, and solvent energy transfer in the vicinity of the solute. VER is usually addressed to the main channel of energy transfer from the solute to the solvent. However, it is quite evident from a general point of view that the latter cannot be considered separately from other accompanying processes, especially in dense solvents.

Unfortunately, even up-to-date experimental techniques provide us only with the vibrational energy relaxation time which, although it is a significant integral characteristics of the phenomenon, is not sufficient to investigate VER in detail. Thus versatile theoretical investigations are of great importance for a profound understanding of VER.

Theoretical methods to consider this complex phenomenon for polyatomic solutes were developed in Ref. 24, hereafter referred to as paper I. They are based on classical molecular dynamics (MD) simulations of equilibrium or nonequilibrium systems comprising one solute and several hundreds of solvent molecules. In turn, mode and atom specific methods were developed to interpret MD simulation data.

Results of nonequilibrium molecular dynamics (NEMD) simulations to directly determine the energy flux from a vibrationally hot molecule to the bath for the case of azulene

[a]Permanent address: Berlarussian State Technological University, 13a Sverdlova Str, 220 050 Minsk, Belarus.
[b]Electronic mail: jschroe2@gwdg.de

dissolved in carbon dioxide or xenon and their detailed analysis were reported in Ref. 25, hereafter referred to as paper II. This analysis revealed a complicated character of the energy redistribution in the solute–solvent system.

The remarkable equipartitioning of the solute vibrational energy among its vibrational degrees of freedom was demonstrated[22,25] while the solute rigid body translations and rotations became thermalized on a subpicosecond time scale. Thus during the relaxation process the solute vibrational subsystem can be represented in terms of its quasiequilibrium state with slowly decreasing temperature. The solute–solvent interactions play an important part in highly efficient intramolecular energy redistribution ensuring the solute quasiequilibrium.

A mode specific analysis has shown[22,25] that solute vibrations from the whole spectral region are active in the solute–solvent energy exchange. However, this energy exchange is not a unidirectional solute-to-solvent process. Some vibrational modes take energy from the cold solvent to the hot solute. These peculiarities of VER are stipulated by complicated inter- and intramolecule dynamics and nonlocality of the potential energy distribution. Although nonequilibrium molecular dynamics (NEMD) simulations shed light on many important features of VER they cannot give a complete description of the phenomenon especially with respect to its statistical mechanical features.

Modern statistical mechanical theories[26–28] allow one to calculate different nonequilibrium characteristics via certain *equilibrium* time correlation functions (TCFs) providing the basis for equilibrium molecular dynamics (EMD) investigations of the corresponding *nonequilibrium* processes. In paper I it was shown that the solute–solvent interaction capacity TCFs are of major importance for the case of VER. Considering the solute vibrations and the solvent as weakly interacting subsystems, these TCFs can be decomposed into the products of solute normal velocity and external normal force TCFs. These three types of TCFs (capacity, force, and velocity) contain the main statistical mechanical characteristics of VER.

Conventional theories[1,4,11,13] of VER are mainly applicable to solutes with one prominent vibrational degree of freedom. They are based on the Landau–Teller formula involving the force TCFs in the form of frequency-dependent friction coefficients. Our approach (see paper I) yields the same result when the velocity autocorrelation function (ACF) is approximated by a harmonic function of time. However, for the multimode problem the velocity and force autocorrelation as well as cross-correlation functions come into play. It was shown in paper I that these functions can be considered either on an atomic or mode specific footing. One may expect that the cross-correlation contributions are less pronounced in the mode specific representation and thus the latter is a more convenient basis for the analysis of VER.

Standard formulations of statistical mechanical theories are concerned with weakly nonequilibrium processes described by linear macroscopic equations. However, a strongly nonequilibrium state of the solute–solvent system is maintained during VER thus requiring an additional substantiation for applicability of the equilibrium approach proposed. The experimentally observed[12,18] exponential excitation energy decays are consistent with a linear energy evolution equation and constitute a first indication of the applicability of our approach.

A second argument appears from the two-temperature model proposed in paper I. This model explains why a weakly nonequilibrium theory can be applied to a strongly nonequilibrium process. The reason lies behind the weak solute–solvent interaction that allows us to introduce the concept of two weakly connected quasiequilibrium subsystems, namely the solute and the bath. Really the bath is almost an equilibrium subsystem while the solute is characterized by a slowly decreasing temperature. The correctness of this representation was proven by direct NEMD simulations in paper II and Ref. 22. The properties of the hot solute involved in VER appear in the velocity TCFs, which can be rescaled to the solvent conditions by a factor proportional to the solute temperature. The properties of the solvent are displayed by the force TCFs (or friction coefficients) and are consistent with its equilibrium state at the bath temperature.

This explanation rests upon some approximations like the scaling hypothesis for the velocity TCFs or the splitting of the capacity TCFs into the product of the velocity and force TCFs. Although these approximations correlate well with a weak solute–solvent interaction, the direct verification of the model by comparing EMD and NEMD simulations is necessary. Thus we have to use the same potential model of the system to be able to make meaningful comparison.

Of course, the same problem of the verification of the applicability of the Landau–Teller formula and equilibrium friction coefficients exists in the case of only a single vibrational mode, also because of the strongly nonequilibrium state of the solute. Again, the main reason why this approach works can be traced to weak solute–solvent interactions. A few successful comparisons of EMD and NEMD simulations for this case are available in the literature.[1,4,11,19]

It was mentioned above that the relaxation time (or rate) represents a very important but only a single characteristic of VER. Analysis of NEMD data in paper II revealed many peculiarities of VER dynamics. This paper is devoted to a detailed investigation of time correlation functions directly connected to VER that substantially complements the NEMD analysis of VER. At the same time, the TCFs examined can be considered in a wider context. Velocity and force TCFs are widely used tools of liquid state theories that in turn are applied[13,29] to investigate VER (see also Ref. 30 and references therein).

Although a particular system (azulene in carbon dioxide) is considered here we believe that mechanisms of VER revealed and discussed in this series of papers are of a more general nature for a class of systems comprising a moderate size solute (toluene, cyclohexene, etc.) and a dense solvent. To the best of our knowledge this type of analysis of VER is represented for the first time.

The outline of the paper is a follows: In Sec. II we briefly review the MD method used. Section III presents a mode specific analysis of azulene dynamics in fluid CO_2. Characteristics of azulene normal vibrations as well as normal mode velocity, force, and capacity time correlation func-

tions are considered. The section closes with an evaluation of the vibrational energy relaxation time. Analogous results on the basis of the atomic coordinate representation are considered in Sec. IV. Section V contains concluding remarks.

II. METHODS

The potential model used for azulene and CO_2 and the technical details of the computer simulations are described elsewhere[21,25] and only the main characteristics are summarized here. We use classical NEV equilibrium molecular dynamics treating both solute and solvent completely flexible. The simulated system consists of one azulene molecule surrounded by CO_2. Periodic boundary conditions are imposed on the simulation box and long-range electrostatic interactions are calculated via the Ewald sum. All simulations were done with the CHARMM package[31] modified to our needs. The potential for azulene and CO_2 and the thermodynamic states considered are as described in paper II. For the azulene–CO_2 system the number of bath molecules was 216 and 337 for low ($\sim$3.2 MPa, $T\cong 445$ K, $\rho=0.93$ mol/ℓ) and high pressure ($\sim$270 MPa, $T\cong 298$ K, $\rho=28.7$ mol/ℓ), respectively, where T and ρ denote the equilibrium solvent temperature and density during the simulation. Equilibrium simulations were performed for each thermodynamic state by generating six trajectories of 396 ps length each as a basis for the calculation of appropriate averages.

The separation of the solute energy E_1 into translational, rotational, and vibrational contributions were done within the Eckart frame (see paper I for details). As shown in paper II the vibration–rotation coupling contribution to the overall energy transfer is less than 1%. Thus, this separation, though not exact, should lead to reliable data for VER.

Spectral representations of different time correlation functions were obtained by fast Fourier transform.[32,33] To improve simulation statistics each trajectory was divided up into segments of 33 ps length providing a spectral resolution of $\sim$1 cm^{-1}. Sampling was every 4 fs (each eighth point in the trajectory at a time step of 0.5 fs) giving a Nyquist critical frequency of 4125 cm^{-1}, well above the highest hydrogen stretch frequencies of azulene at about 3000 cm^{-1}. All Fourier transforms calculated in this way already drop to zero at $\sim$3500 cm^{-1}.

III. NORMAL MODE ANALYSIS

According to our analysis in paper I and the results of paper II indicating a negligible contribution of vibration–rotation interaction to VER, Eq. (3.27) of paper I can be used for the transfer rate k_{vibr},

$$k_{\mathrm{vibr}}=\frac{1}{c_1 k_B T^2}\int_0^\infty \langle N_{\mathrm{vibr}}(t)N_{\mathrm{vibr}}(0)\rangle dt, \tag{1}$$

where brackets $\langle\ \rangle$ indicate ensemble average, c_1 denotes the thermal capacity of the solute, and N_{vibr} is the vibrational capacity of the solute–solvent interaction calculated for a solute molecule of n vibrational degrees of freedom as

$$N_{\mathrm{vibr}}(t)=\sum_{\alpha=1}^{n} N_\alpha(t)=\sum_{\alpha=1}^{n} Q_\alpha(t)\dot{q}_\alpha(t) \tag{2}$$

with $N_\alpha(t)$, $Q_\alpha(t)$, and $\dot{q}_\alpha(t)$being the capacity, generalized external force on, and velocity of mode α at time t, respectively. Thus the energy transfer rate is represented by the time integral over the vibrational capacity TCF, which in turn consists of the sum of all matrix elements produced by insertion of Eq. (2) into Eq. (1),

$$k_{\mathrm{vibr}}=\sum_{\alpha,\beta}^{n} k_{\alpha\beta}, \tag{3}$$

$$k_{\alpha\beta}=\frac{1}{c_1 k_B T^2}\int_0^\infty \langle N_\alpha(t)N_\beta(0)\rangle dt. \tag{4}$$

Under the assumption that the normal mode velocity and force[34] can be decoupled (see paper I) the last expression can be rewritten in the form

$$k_{\alpha\beta}=\frac{1}{c_1 k_\theta T^2}\int_0^\infty \langle Q_\alpha(t)\dot{q}_\alpha(t)Q_\beta(0)\dot{q}_\alpha(0)\rangle dt$$

$$\cong\frac{1}{c_1 k_B T^2}\int_0^\infty \langle Q_\alpha(t)Q_\beta(0)\rangle\langle \dot{q}_\alpha(t)\dot{q}_\beta(0)\rangle dt, \tag{5}$$

introducing the time autocorrelation (at $\alpha=\beta$) and cross-correlation (at $\alpha\neq\beta$) functions of normal forces and velocities.

It is evident from Eqs. (1) and (5) that a solute with more than one vibrational degree of freedom cannot be considered as a collection of independent normal mode oscillators due to contributions from the cross terms. It was shown in paper II and Ref. 22 that each solvent molecule–solute atom interaction contributes to several normal forces simultaneously that should result in comparable values of diagonal autocorrelation and nondiagonal cross-correlation functions of normal forces. However, for an isolated harmonic solute its normal velocity cross-correlation functions vanish and intermode coupling can arise through normal mode disturbances due to external forces resulting in that the cross velocity TCFs appear as the main indicators of the intermode coupling with respect to VER. Thus, in the following sections, we analyze properties of different TCFs involved in the energy transfer process according to Eqs. (1)–(5).

A. Azulene normal mode characteristics

Before starting the analysis of different TCFs it is useful to sketch the main features of the azulene normal modes. Apart from the symmetry represented in Table I a subdivision into local and global normal modes is also possible. Of course, the latter is rather ambiguous as there are many modes that are intermediate in character. However, all low frequency modes up to No. 17 can be called global as their eigenvectors have components significantly different from zero for all or almost all azulene atoms. Some global modes like vibrations 1, 2, 4, and 6 (see Fig. 1) are characterized by smooth change in displacements of neighboring nuclei. They reflect motions of the azulene rings as quasirigid objects. At higher eigenfrequencies even nearest-neighbor nuclei can move in opposite directions (e.g., modes 20 and 48). Among the high frequency C–H stretches only vibrations 44, 46, and 48 belong to global modes.

TABLE I. Symmetry assignment of normal modes and their calculated frequencies. [The following abbreviations are used: in-plane symmetric (ips), in-plane asymmetric (ipa), out-of-plane symmetric (ops), out-of-plane asymmetric (opa).]

Mode number	Frequencies (cm^{-1})				Mode number	Frequencies (cm^{-1})	
	opa	ops	ipa	ips		ipa	ips
1	185				26		1029
2		238			27	1041	
3		327			28	1067	
4			330		29	1130	
5	392				30		1174
6				395	31	1224	
7			434		32	1296	
8		545			33		1398
9	554				34	1420	
10				582	35	1480	
11		588			36		1496
12				745	37	1528	
13			759		38		1578
14				785	39		1598
15		789			40	1642	
16	852				41		3028
17		859			42	3028	
18			866		43		3031
19		916			44	3034	
20	948				45		3036
21		967			46	3036	
22				967	47		3036
23	999				48		3039
24				1016			
25		1027					

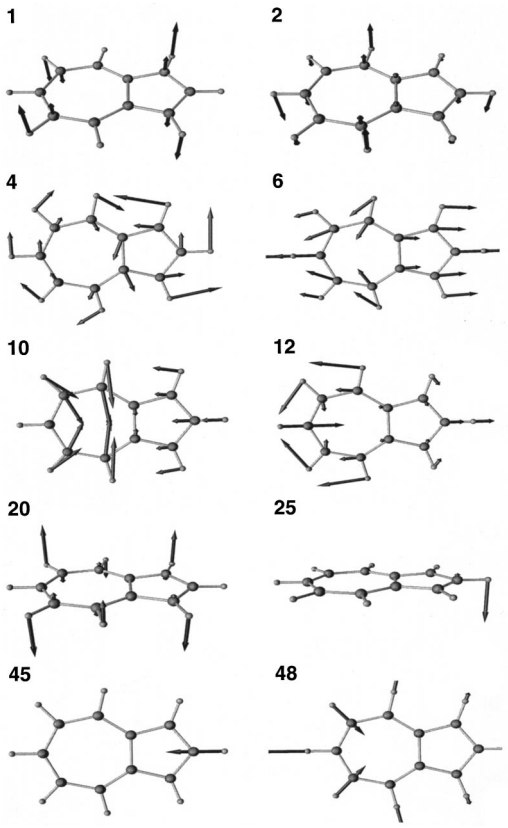

FIG. 1. Eigenvectors of particular azulene normal modes as indicated by mode numbers. For each mode, projections of arrows on coordinate axes determine all 48 eigenvector components in arbitrary units. The eigenvector components of out-of-plane modes (1, 2, 20, and 25) are perpendicular to the azulene plane.

Several normal modes (namely, modes 18, 32, 33, 34, 35, 38, 39, 40, 41, 42) can be ascribed to partially global excitations because mainly atoms of one ring or other small groups of atom show considerable displacements. Eigenvectors of local modes 19, 25, 28, 43, 45, 47 have significant components for one, two, or three atoms.

Amplitudes of nuclei displacements and velocities attributed to a given mode are proportional to the length of the respective arrows shown for particular modes in Fig. 1. The normalization conditions

$$\sum_{i=1}^{n_s} m_i \dot{q}_{i\alpha}^2 = k_B T, \tag{6}$$

$$\sum_{i=1}^{n_s} m_i q_{i\alpha}^2 = k_B T/\omega_\alpha^2, \tag{7}$$

where n_s is the number of solute atoms, indicate that the higher the frequency the lower the displacements $q_{i\alpha}$ of nuclei i arising due to the αth normal mode vibration, while velocity amplitudes do not depend on normal mode frequency ω_α. For azulene the square of the ratio between the highest and the lowest frequencies is greater than 200. Again, the more nuclei that are involved in a given vibration the lower the values of their characteristic velocities and displacements. The role of nuclei masses are also evident from Eqs. (6) and (7), and big weight coefficients of carbon nuclei strongly reduce the normal mode vibrational displacements and velocities when carbon components are significant.

Nuclei displacements are of major importance for an intuitive understanding of the strength of the normal mode interaction with a dense solvent. For example, the group of modes 15–34 is characterized by low values of carbon components that in view of Eq. (7) in part compensate for the frequency increase with respect to modes 1–14, thus giving an explanation for their relative significance in the solute to solvent vibrational energy transfer. Comparatively low activity of in-plane modes 4, 6, 7, 10, 13, 14 (see Fig. 3 in paper II) can be attributed to their eigenvector structures with large components of C nuclei.

B. Velocity time correlation functions

For a harmonic system the normal mode velocity TCFs are characterized by a single peak at the eigenfrequency of the respective vibration. However, the kinematic anharmonicities present in polyatomic molecules (see paper II) and interactions with the bath can be expected to influence the spectral pattern and linewidths of the mode spectra.

In Fig. 2 spectra of the velocity autocorrelation function

$$V_\alpha^2(\omega) = \frac{1}{k_B T}\int_{-\infty}^{\infty} \exp(i\omega t)\langle \dot{q}_\alpha(t)\dot{q}_\alpha(0)\rangle dt \tag{8}$$

for several modes at different conditions are shown. All spectra are dominated by one peak at the eigenfrequency ω_α of the respective vibration, indicating that the normal mode

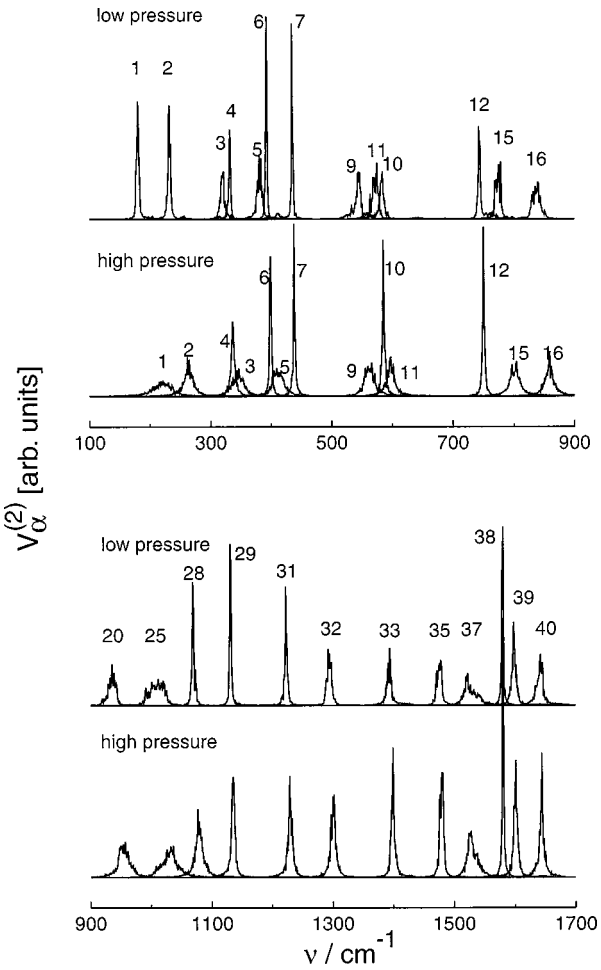

FIG. 2. Spectra of normal mode velocity ACFs for azulene in CO_2 at low (3.2 MPa, $T=445$ K) and high (270 MPa, $T=298$ K) pressure. Mode numbers are indicated at each curve. Due to the blueshift of out-of-plane bands the sequence of modes changes at high pressure.

picture can be used to represent azulene dynamics under the given conditions. As a rule, due to stronger interaction with the bath these peaks are broadened and slightly blueshifted[35] at higher pressure. These effects are pronounced for out-of-plane modes. The frequency shift is about 35 cm^{-1} for the first mode, 10–20 cm^{-1} for the other out-of-plane modes, and negligible for in-plane modes. Because of differences in the behavior of in- and out-of-plane vibrations, transpositions of several modes with close frequencies (e.g., 3 and 4, 5 and 6, 10 and 11) appear at high pressure. Although a tendency exists that the most diffuse bands in the velocity TCFs belong to the lowest frequency modes (e.g., modes 1, 2, 3, and 5) there are exceptions as the highly diffuse bands for local modes 25 and 37 reveal the role of the eigenvector structure.

The spectral shape of many in-plane modes, e.g., 4, 6, 7, 29, and 31 only weakly depends on thermodynamic conditions. Even at 270 MPa the spectra of these modes maintain a sharp structure. Moreover, some in-plane modes like 10, 12, 32, 33, 35, 38, 39 and 40 even exhibit additional narrowing at high pressure. Most of them are symmetric modes. This phenomenon can be attributed to the competing effects of temperature and density (or pressure) of the system. With decreasing temperature the contribution of kinematic nonlinearities decreases, leading to less diffuse spectra of modes that are weakly coupled to the bath. As an example we consider the structure of the tenth mode eigenvector (see Fig. 1). Almost all carbon nuclei contribute to Eq. (7), resulting in small mean square displacements. Moreover, the in-plane nearly radial motion the majority of H nuclei suggests that this motion weakly disturbs interactions of the nuclei with the solvent. In-plane motions of the carbon atoms are well isolated from the solvent influence, too. Another example is mode 38, whose eigenvector mainly consists of stretch vibrations of the bridge carbon atoms.

However, not all in-plane vibrations are insensitive to changes of pressure. For example, the spectra of modes 28 and 37, both in-plane asymmetric, are broadened substantially at 270 MPa. This behavior can be traced to the structure of the respective eigenvectors that have their main contribution from a single hydrogen atom. Therefore, these vibrations, despite being oriented in plane, are sensitive to the change in density because the hydrogen atoms, located in peripheral regions of the azulene molecule, are coupled strongly to the bath. This feature is displayed in spectra of all high frequency hydrogen stretch modes (not shown) 41–48, especially local modes 43, 45, and 47 whose eigenvectors are characterized by high amplitude vibrations of a few H atoms. We note that the largest components of eigenvectors of modes 28, 37, and 45 correspond to in-plane displacements of the H atom that is connected the end C atom of the small and thus more rigid azulene ring. The eigenvector of the highest frequency out-of-plane mode 25 is almost completely represented by vibrations of this hydrogen atom and its broad spectrum is notable even among the out-of-plane mode spectra.

In addition to this, different vibrations like 9, 16, 25, or 37 lead to diffuse bands even at low pressure. Modes of this type split up into two groups. On the one hand, for vibrations 25 and 37 the previous discussion holds, as the main contribution comes from a single H atom. Thus, even a weak perturbation at low pressure together with the temperature factor leads to a broadening of the respective spectra. On the other hand, vibrations like 9 and 16 are closely related to the properties of mode 1, described as asymmetric out of plane. As discussed below, such vibrations are strongly correlated with each other.

Thus the properties of the velocity ACFs weakly depend on temperature and are mainly determined by the solute–solvent interaction as well as the internal solute eigenvector structure. To underline this fact, we show in Fig. 3 spectra[36] of the velocity cross-correlation functions calculated as

$$V_{\alpha,\beta}(\omega)=\frac{1}{k_BT}\int_{-\infty}^{\infty}\exp(i\omega t)\langle\dot{q}_\beta(t)\dot{q}_\alpha(0)\rangle dt. \tag{9}$$

For modes of different symmetry (1 and 11, 1 and 13, 3 and 9, 3 and 13, see Table I), the spectra consist mainly of two noisy disturbances at the eigenfrequencies of the contributing vibrations, whereas for modes of the same symmetry (1 and 9 or 5 and 9) they show a well-defined structure because of the significant correlation between vibrations. Again, out-of-plane vibrations show stronger mutual correlations even if

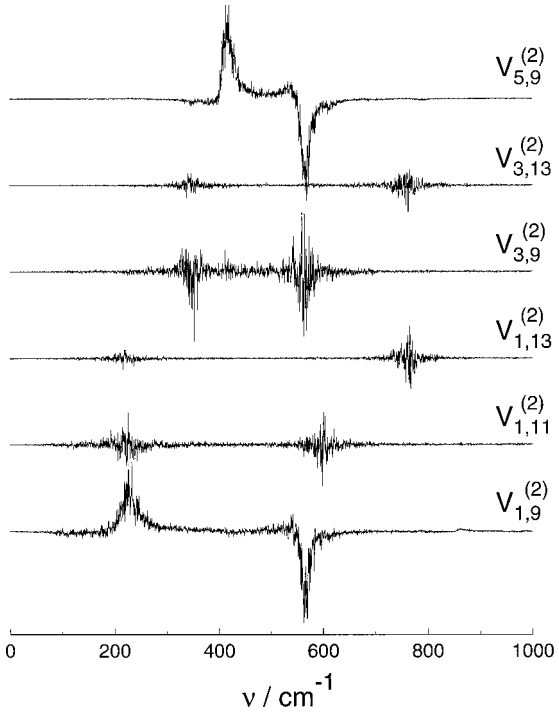

FIG. 3. Fourier transforms of the velocity cross-correlation functions for azulene in CO_2 at high (270 MPa) pressure.

they are of different symmetry (e.g., symmetric mode 3 and asymmetric mode 9) as compared to other combinations of symmetry indicators (modes 1 and 11, 1 and 13, 3 and 13, see Table I).

Several physical factors could be responsible for the observed features of the velocity TCFs. On the one hand, the solute molecule is exposed to the fluctuating potential field of the surrounding solvent. This results in the spectral blueshift previously mentioned of modes that are most sensitive to the solvent influences, i.e., mainly of out-of-plane modes. Again, thermal fluctuations of the force field lead to the broadening of the spectra with increasing pressure.

On the other hand, the solute and the nearest solvent molecules' temporal clusters possess their own mode structure that includes slightly modified eigenvectors of isolated azulene. In turn, spectra of these clusters consist of slightly modified isolated solute bands and the low frequency contributions due to weak solute–solvent interactions that can be attributed to the bath normal modes. The modified eigenvectors are composed of linear combinations of the isolated solute eigenvectors and additional components belonging to solvent molecules with respective weight coefficients. The main contribution to the solute part of a temporal cluster eigenvector is made up by its prototype is the isolated solute. Accordingly, the time evolution of a solute normal mode velocity may be represented as a linear combination of all vibrations

$$\dot{q}_\alpha(t) = \sum_{\gamma=1}^{s} u_{\alpha\gamma} \cos(\omega_\gamma t + \delta_{\alpha\gamma}), \tag{10}$$

where the sum is taken over all vibrational degrees of freedom of the solute, $\delta_{\alpha\gamma}$ and $u_{\alpha\gamma}$ are fluctuating phases and amplitudes of the respective harmonics. The damping of vibrations and coupling to low frequency solvent modes are disregarded here.

Mode γ is a generating factor, which — induced by the solvent — gives rise to harmonic contributions with frequency ω_γ to different vibrations α. Moreover, solute vibrations are able to create structures of their own symmetry in the solvent, giving rise to pronounced intermode correlations. Thus the indices α and γ are not symmetric and substantial correlations can be expected only between the amplitudes or phases with coinciding second indices.

As discussed above, the diagonal velocity amplitudes $u_{\alpha\alpha}$ considerably surpass nondiagonal ones. The consequences of solvent assisted solute intermode coupling, leading to Eq. (10), are considered in the Appendix. There it is shown that the strength of the intermode correlations can be estimated by integration of the velocity cross-correlation spectra from zero to one-half the sum of the eigenfrequencies of the modes under consideration. For noticeably correlated modes (such as 1 and 9, 5 and 9) these integrals amount to about 1% of the integrals over the spectra of velocity ACFs. Thus even for such modes cross-correlations are rather weak. In other cases the strength of correlations is even lower by an order of magnitude or more. At low pressure the normal mode velocity cross-correlation spectra are very weak and hardly noticeable on the background of fluctuations.

C. Force time correlation functions

For the normal force friction coefficients as defined by the Fourier transform of the ACF of the fluctuating normal force $Q_\alpha(t)$ exerted on azulene by the surrounding medium,

$$F_\alpha^{(2)}(\omega) = \frac{1}{k_B T} \int_{-\infty}^{\infty} \exp(i\omega t) \langle Q_\alpha(t) Q_\alpha(0) \rangle dt, \tag{11}$$

differences between low and high pressure data are also pronounced.

As shown in Fig. 4, at 3.2 MPa $F_\alpha^{(2)}(\omega)$ has a similar shape for all modes. After a fast initial rise the function reaches its maximum at $\sim$20 cm^{-1}. For higher frequencies it decays almost exponentially up to $\sim$500 cm^{-1}. Weak manifestations of the eigenfrequencies of other modes are observable only for vibrations 1 and 2. Differences in symmetry for different modes are manifested in the intensities of the respective spectra. In-plane modes (e.g., mode 4) usually show much lower intensities than out-of-plane modes of comparable eigenfrequency. This effect is also observed at high density where lower intensity spectra are also connected to in-plane motions within the azulene molecule. Nevertheless, the overall appearance of the spectra is rather different under these thermodynamic conditions. At 270 MPa the $F_\alpha^{(2)}(\omega)$ decay cannot be described as monoexponential. It consists of a fast decaying component followed by a slowly declining tail. For many higher frequency vibrations like modes 9 or 16 the force ACFs display some structural features in the low frequency range (below 200 cm^{-1}). In addition to this, prominent peaks with decreasing intensity at increasing frequencies are observable at ω_α for most of the vibrations, indicating that at high pressure vibrations are directly

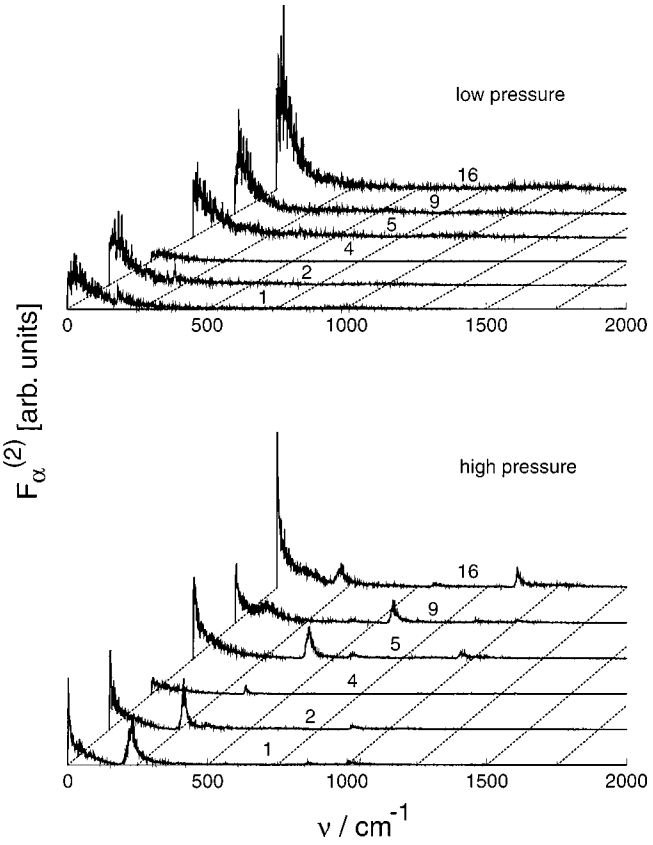

FIG. 4. Fourier transforms of the normal force ACFs for azulene in CO_2 at low and high pressure. Mode numbers are indicated at each curve.

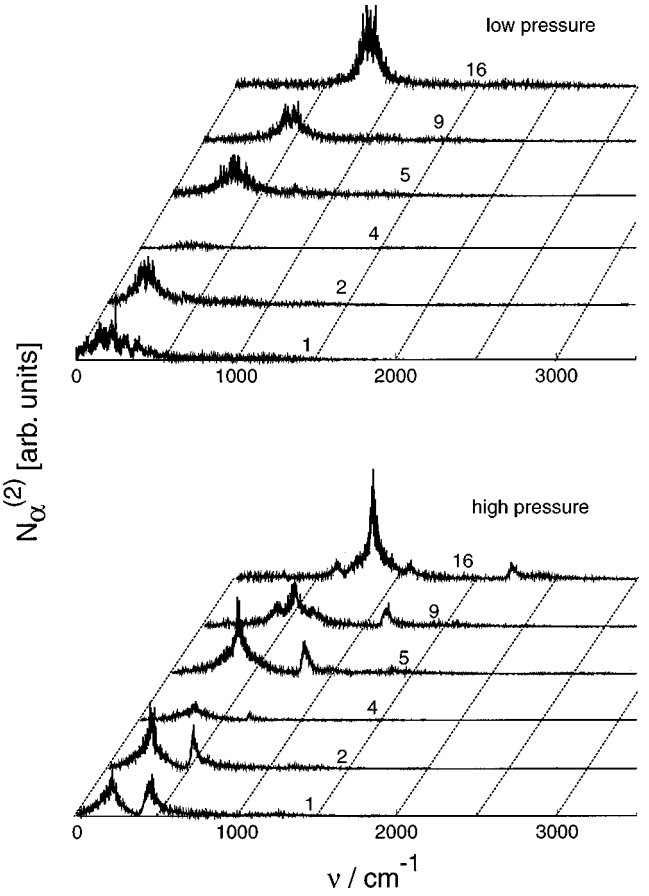

FIG. 5. Fourier transforms of the capacity ACFs for azulene in CO_2 at low and high pressure. Mode numbers are indicated at each curve.

coupled to the bath. However, for specific vibrations, like mode 16, in addition to the contribution of the eigenfrequency to the spectrum here is a signal at the frequency of the lowest vibrational mode due to the same symmetry of these modes. As for the velocity ACFs this behavior can be attributed to the intermode coupling in cases of a similar eigenvector structure.

D. Capacity time correlation functions

Spectra of the normal mode capacity ACFs

$$N_\alpha^{(2)}(\omega)=\int_{-\infty}^{\infty}\exp(i\omega t)\langle\dot{q}_\alpha(t)Q_\alpha(t)\dot{q}_\alpha(0)Q_\alpha(0)\rangle dt \tag{12}$$

display properties of fluctuating normal forces as well as velocities. The spectra observed at 3.2 MPa differ strongly from the high pressure result (see Fig. 5). At low density the structure of the spectra can approximately be described as a broad Gaussian signal centered at ω_α, while at 270 MPa the spectra are dominated by two peaks: a first one, as in the low pressure case, at the eigenfrequency of the respective mode but with sharper structure, and a second at $2\omega_\alpha$ showing an asymmetric structure. As was shown in the velocity and force autocorrelations, this frequency doubling is due to contributions of the mode eigenfrequency both to the velocities and the external forces under these thermodynamic conditions. The intensity of the second peak decreases in comparison with the first one at increasing ω_α because of a declining contribution from force autocorrelations at high frequencies. As in the previous cases, signals of lower intensity are calculated for in-plane vibrations at both pressures.

E. Vibrational energy relaxation rate

Considering that cross correlations only to a small extent contribute to the process of energy relaxation, in a first approximation the relaxation rate [Eqs. (3) and (4)] can be calculated from diagonal elements of the capacity correlation matrix

$$k_{\mathrm{vibr}}\cong\sum_{\alpha=1}^{3n_s-6}k_{\alpha\alpha}=\frac{1}{c_1k_BT^2}\sum_{\alpha=1}^{3n_s-6}\int_0^\infty\langle N_\alpha(t)N_\alpha(0)\rangle dt$$
$$=\frac{1}{48(k_BT)^2}\sum_{\alpha=1}^{3n_s-6}N_\alpha^{(2)}(0), \tag{13}$$

where we use the harmonic approximation for the heat capacity of the azulene vibrational subsystem. From simulation data this approximation was found to be quite accurate. Thus, the value of the capacity ACF at $\omega=0$ should give an estimation of the contribution of a specific mode to VER. At 3.2 MPa $N_\alpha^{(2)}(0)$ decreases rapidly with increasing ω_α indicating that only the lowest frequency modes contribute sub-

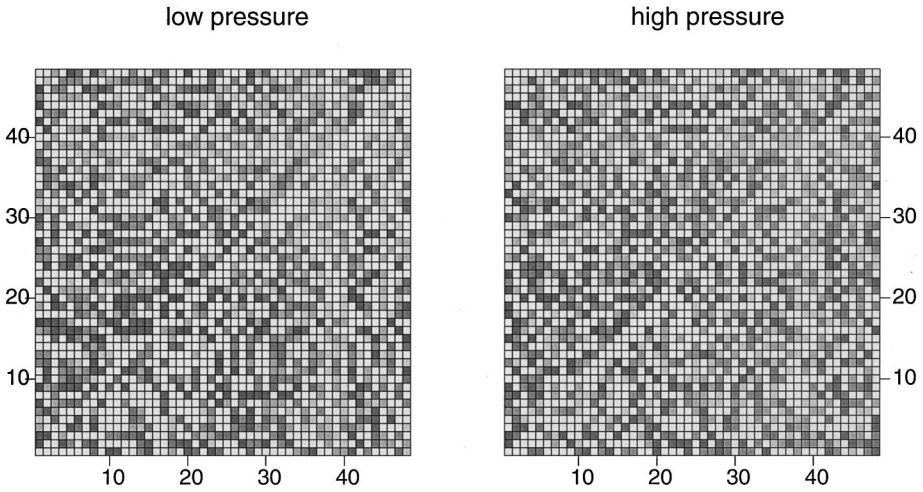

FIG. 6. The gray shade coded distribution of absolute values of the capacity cross-correlation matrix elements for azulene in CO_2 at low and high pressure. Mode numbers are indicated among the coordinate axes. The diagonal matrix elements are set to zero. Values of the positive and absolute values of the negative matrix elements are shown below and above this diagonal, respectively. The darkest points correspond to relaxation rates 2.5×10^7 and 5×10^8 s^{-1} for low and high pressure, correspondingly.

stantially to the overall process. At high pressure, however, even high frequency modes are active. These observations agree with results from our nonequilibrium simulations in paper II showing that in a dense environment almost all modes are participating in energy transfer to the bath. The relaxation rates calculated from Eq. (13) correspond to relaxation times ($\tau=1/k_{\mathrm{vibr}}$) of 120 and 6 ps for 3.2 and 270 MPa, respectively, significantly smaller than the values obtained from the nonequilibrium simulations of 306 and 12.5 ps. Therefore, the overall contribution of the cross terms to the relaxation rate cannot be neglected, as one could expect from the velocity cross-correlation functions.

We have calculated the zero frequency values $N^{(2)}_{\alpha\beta}(0)$ for capacity cross correlations at low and high pressure. The resulting coupling matrices normalized according to Eq. (4) are displayed in Fig. 6. All diagonal elements in Fig. 6 are set to zero because many of their values are an order of magnitude higher than the largest nondiagonal elements.

The intermode coupling at both pressures is well pronounced although the coupling strength decreases with increasing frequency of at least one of the correlated modes. However, the hydrogen stretch vibrations are strongly correlated among each other as well as to the other modes. This intermode energy exchange is essential for the fast internal thermalization of azulene during vibrational relaxation that was observed in nonequilibrium simulations.[22,25]

Different signs of the matrix elements indicate that the respective coupling enhances or reduces the overall VER rate for positive or negative contributions, respectively. The greater number of dark points in the upper left-hand parts of the squares in Fig. 6 indicate that the overall contribution of the negative matrix elements is greater than that of the positive ones, thus reducing the vibrational relaxation rate. Therefore, a calculation of relaxation rates on the basis of Eq. (13) can only serve as a rough approximation to the multimode problem.

For a proper estimation of the relaxation rate the cross-correlation contributions have to be taken into account. However, the evaluation of time integrals over correlation functions by means of a Fourier transform implies using the zero frequency limit. Our calculations have shown that the available frequency resolution and statistics of the simulated data can be used for semiquantitative estimation of the matrix elements displayed in Fig. 6, but are not sufficient for a precise investigation of the relaxation rates. To circumvent these obstacles, we recalculate k_{vibr} according to Eq. (3) as

$$k_{\mathrm{vibr}}=\sum_{\alpha=1}^{n} k_\alpha, \tag{14}$$

considering each term here as the contribution of mode α to the relaxation rate

$$k_\alpha=\sum_{\beta=1}^{n} k_{\alpha\beta}=\frac{1}{c_1 k_B T^2}\int_0^\infty \langle N_\alpha(t) N_{\mathrm{vibr}}(0)\rangle dt. \tag{15}$$

Integrating capacities we rewrite this expression in terms of energies $W_\alpha(t)$ and $W_{\mathrm{vibr}}(t)$,

$$W_\alpha(t)=\int_0^t N_\alpha(t')dt', \quad W_{\mathrm{vibr}}(t)=\int_0^t N_{\mathrm{vibr}}(t')dt', \tag{16}$$

transferred for the solute to the bath during time t by αth mode and by all vibrational modes, respectively, and represent the partial relaxation rates through Helfand integrands[37,38]

$$k_\alpha=\frac{1}{2c_1 k_B T^2}\lim_{t\to\infty}\frac{d}{dt}\langle W_\alpha(t) W_{\mathrm{vibr}}(t)\rangle. \tag{17}$$

Equation (17) offers the possibility to represent the expression under the time derivative by a linear fit, thereby smoothing fluctuations caused by poor statistics. Also, data for the total transferred energy $W_{\mathrm{vibr}}(t)$ are more reliable than each particular contribution to it.

In addition, Helfand integrands were used to calculate the vibrational relaxation rate,

$$k_{\mathrm{vibr}}=\frac{1}{96(k_B T)^2}\lim_{t\to\infty}\frac{d}{dt}\langle W^2_{\mathrm{vibr}}(t)\rangle. \tag{18}$$

In Figs. 7 and 8 we plot relaxation rates for individual modes and the accumulation of the rate for all modes $i\leqslant n$ against n for low and high pressure. The time dependencies of the Helfand integrands for the total energy transferred and that

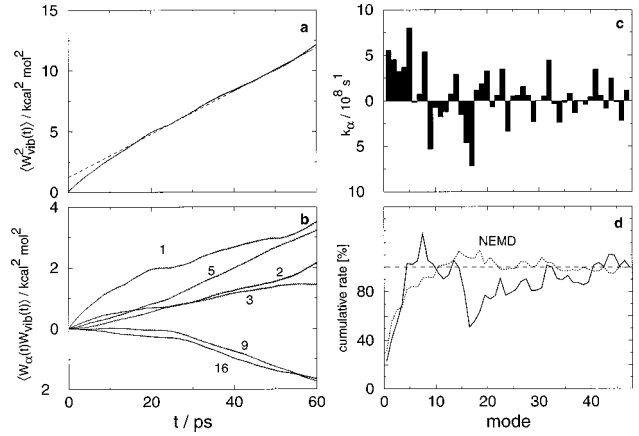

FIG. 7. Relaxation rates for azulene in CO_2 at low (3.2 MPa) pressure. Helfand integrands for the total (a) and partial (b) relaxation rates. The distribution of the partial (c) and cumulative (d) relaxation rates.

entering the expression for the partial relaxation rates are shown for several individual modes. After an initial period that reflects memory effects, the total energy transfer integrands show quite reasonable linear character. Higher fluctuations are observed for the partial integrands. Still they permit the estimation of partial relaxation rates. Time intervals [20,60] ps and [20,40] ps for low and high pressure, respectively, were used for these estimations.

In agreement with nonequilibrium calculations in paper II and Ref. 22, at 3.2 MPa only 5–10 low frequency vibrational modes contribute significantly to the overall energy transfer process, whereas the activity of the other modes results mainly in intramolecular energy redistribution. At high densities almost all modes with exception of the C–H stretches contribute to the energy flux to the bath. The total relaxation rates k_{vibr} amount to 426 and 19.2 ps at low and high pressure, respectively, agreeing reasonably well with our nonequilibrium simulations in paper II where VER times of 306 and 12.5 ps were obtained. However, as noted in paper II, the rate of energy transfer progressively decreases in the nonequilibrium simulations (hence, the relaxation time increases) as the temperature of the solute becomes lower. The estimated relaxation time in high pressure NEMD simulations taking into account this effect was found to be 19.1 ps, which can be compared with the present EMD (19.2 ps) and experimental[18] (18.7 ps) results.

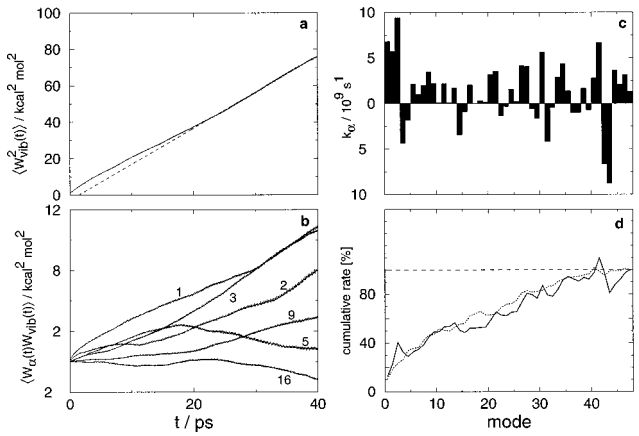

FIG. 8. The same as in Fig. 7 at high (270 MPa) pressure.

An excellent agreement between EMD and low temperature NEMD simulation results is not surprising because the same potentials were used in both cases, thus validating the former approach. However, the relaxation rate as determined from NEMD simulations weakly depends on the solute temperature. Minor differences between the relaxation rates in EMD and high temperature NEMD simulations indicate that equilibrium and quasiequilibrium TCFs are not identical. Still these differences are not significant and EMD simulations at the solvent equilibrium temperature reflect the real nonequilibrium situation at least qualitatively.

In spite of some disagreement between partial relaxation rates calculated by means of NEMD and EMD simulations the general behavior of the cumulative energy fluxes shown in Figs. 7(d) and 8(d) is very similar. Due to shorter relaxation times at high pressure, MD simulations were available with better statistics. Therefore, at high pressure fluctuations, as well as deviations between NEMD and EMD, results are considerably lower.

It is necessary to note that the EMD partial relaxation rates calculated in accordance with Eq. (17) and the energies transferred by particular modes in NEMD simulations [Eq. (16) of paper II], although very similar from an intuitive point of view, still cannot be identified exactly with each other. The cross-correlation contributions $k^{(2)}_{\alpha\beta}$ defined by Eq. (4) reflect the influence of other modes on the energy exchange through a particular mode. However, their interpretation as well as the interpretation of the EMD partial relaxation rates and the energies transferred by particular modes in NEMD simulations in terms of local energy fluxes is ambiguous due to the nonlocality of the interaction energy. The azulene intramolecular potential consists of two-, three-, and four-body interactions which, due to kinematic nonlinearities and solute–solvent interactions, give rise to intermode coupling terms after the transformation to normal mode coordinates. Thus VER and intramolecular vibrational energy redistribution (IVR) cannot be separated from each other and have to be considered as mutually connected processes ensuring an efficient energy decay of the solute.

In Sec. III B it was shown that the normal mode representation is well founded for solutes of the azulene type. Even in high density solvents like carbon dioxide at 270 MPa the energy exchange rates are quite low in comparison with characteristic vibrating time scales. During a relaxation time of an order of 10 ps a mode with frequency as low as 200 cm^{-1} completes about 100 vibrations, dissipating only about a percent of the mode energy per each vibration. Of course, under these conditions the solute motions preserve a well-define mode structure as demonstrated by the spectra of normal mode velocity TCFs.

However, the energy fluxes, although small in comparison with the mode energies, consist of intra- and intermolecular contributions, which cannot be separated from each other due to the nonlocality of the interaction energy discussed previously. This complicated character of the energy exchange manifests itself by significant differences between

different mode energy fluxes in NEMD as well as by nonzero values of the nondiagonal energy exchange matrix elements in EMD simulations. The nondiagonal matrix elements are an order of magnitude lower than the diagonal ones. This indicates that the effective intermode energy exchange between two particular modes on average is one order of magnitude smaller than the energy exchange between a particular mode and the solvent. Thus the cumulative energy exchange of a particular mode with all other coupled solute modes can compete with the energy transfer from this mode to the solvent, leading to fast IVR if there is a sufficient number of solute vibrational degrees of freedom as in the case of azulene.

IV. ATOM SPECIFIC ENERGY TRANSFER

A. Atomic time correlation functions

In contrast to the normal mode case each atomic velocity ACF spectrum consists of a variety of signals related to contributions of different normal vibrations that strongly depend on the position of the atom in azulene in accordance with the structure of eigenvectors. For example, C–H stretch vibrations are displayed in spectra of all C nuclei but the third one (see Ref. 21 for the assignment of atoms) that is in a bridge position and not directly connected to hydrogen atoms. The competition between decreasing temperature and rising pressure that was already discussed in Sec. III B, enhances the resolution of atomic spectra at high pressure.

The frequency-dependent atomic friction coefficients $F_i^{(2)}(\omega)$ were calculated as the Fourier transforms of the atomic force TCFs. At low pressure they show similar structure of broad distorted Gaussians centered at $\sim 100\ \mathrm{cm}^{-1}$ for all C and H nuclei. The third bridge carbon atom being mostly isolated from the solvent is characterized by comparatively low intensity spectra at both pressures. In the high frequency range H nuclei exhibit connection with different normal vibrations. At high pressure the low frequency maximum is displaced to higher frequencies and azulene eigenfrequencies, especially the lowest one, manifest themselves by respective peaks indicating stronger solute–solvent interactions.

From $F_i^{(2)}(\omega)$ three different types of C atoms can be distinguished at both pressures. First, C nuclei 1 and 2, which form the core of the five-membered ring in azulene, show the highest intensities because due to the small bending angle within the molecule ($\sim 110°$) these atoms are in closest contact with the solvent; second, the bridge nuclei C_3, shielded in the center of the solute, are coupled only weakly to the bath leading to low intensity spectra; and third, the core atoms of the seven-membered ring with intermediate intensities. Differences between hydrogen nuclei are much less pronounced. For a given pressure the calculation of $F_i^{(2)}(\omega)$ leads to comparable results for all H atoms, indicating that due to their location in the peripheral regions of the solvent all of them experience the same interacting with the solvent.

For the atomic capacity ACFs $N_i^{(2)}(\omega)$ a change in density leaves their spectral shape almost unaffected. Despite the different intensities, $N_i^{(2)}(\omega)$ keeps its basic structure over two orders of magnitude in pressure. For carbon nuclei one can see wide bands from zero frequency to approximately $1500\ \mathrm{cm}^{-1}$ with numerous peaks on the background of slowly decreasing amplitude, and weak contributions of C–H stretches at $\sim 3000\ \mathrm{cm}^{-1}$. It is produced by a collection of normal mode contributions shown in Fig. 5. In accordance with Fig. 5, peaks are more pronounced at high pressure. Again, the structure of $N_i^{(2)}(\omega)$ closely reflects the location of the atoms and three different classes of nuclei can be distinguished from the spectra. For C nuclei 1 and 2, which belong to the five-membered ring dominated by low frequency out-of-plane motions and, due to its rigid structure, high frequency ring deformations at $\sim 1500\ \mathrm{cm}^{-1}$ $N_i^{(2)}(\omega)$ slowly decays up to $1000\ \mathrm{cm}^{-1}$ and then sharply drops in intensity. In the following, peaks are observed around $1500\ \mathrm{cm}^{-1}$. Consequently, for atoms C_4, C_5, and C_6 main intensity is redshifted to $1000\ \mathrm{cm}^{-1}$ where the deformations of the larger, floppier ring are located. In contrast to this, the spectra for C_3 nuclei have low intensity in the low frequency range below $500\ \mathrm{cm}^{-1}$ due to the position of these nuclei on the rigid bridge that connects the two rings and does not contribute to most low frequency out-of-plane motions.

All capacity autocorrelation spectra for hydrogen nuclei are dominated by two broad peaks around $1000\ \mathrm{cm}^{-1}$ and at the frequency of the hydrogen stretch vibrations ($\sim 3000\ \mathrm{cm}^{-1}$). In agreement with our nonequilibrium simulations, intensities are by a factor of 5 higher in comparison to the carbon spectra, indicating that most of the energy is transferred through the H atoms. As for the friction coefficients only small differences between the capacity spectra of different hydrogen nuclei can be found.

B. Energy relaxation rates

In analogy to the normal mode analysis, atom specific relaxation rates can be calculated according to Eqs. (13)–(17), where now the capacity $N_i(t)$ and the energy $W_i(t)$ transferred through atom i instead of the mode specific quantities have to be substituted and the summations are carried out over all azulene nuclei.

The calculation of the capacity ACFs $N_i^{(2)}(\omega)$ already indicated that the hydrogen atoms are most active agents in the energy exchange with the bath. The evaluation of the energy transfer rates supports this observation. In Fig. 9 atomic partial rates for all azulene nuclei are shown. Contributions of carbon nuclei in and adjacent to the bridge are extremely low. These nuclei do not actively participate in out-of-plane motions.

Of course, the overall contributions can be decomposed into diagonal and nondiagonal parts. The nondiagonal parts for the bridge and big ring carbon atoms are almost exactly equal to the diagonal contributions but with negative sign, thus resulting in almost vanishing activity with respect to energy transfer. Zero activity of atoms in the big ring close to the bridge is compensated by high activity of hydrogen atoms bonded to them, especially at high pressure. The distribution of the energy transferred among different atoms (Fig. 9) is more inhomogeneous in comparison with NEMD results. However, the ratios of the energies transferred by all

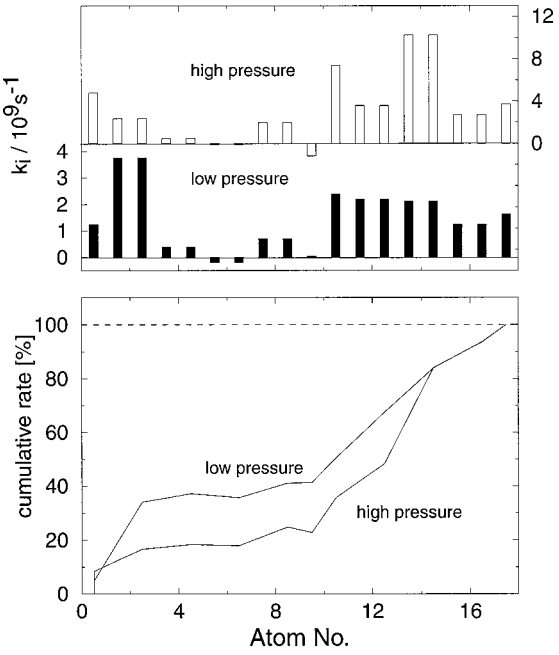

FIG. 9. Atomic partial and cumulative relaxation rates. Carbon atoms are numbered from 1 to 10 beginning from the end atom of the small azulene ring and numbering symmetrically placed atoms by a couple of successive numbers: 2 and 3, 4 and 5, etc., 4 and 5 are bridge atoms. Hydrogen atoms are numbered in the same order (11, 12 and 13, etc.).

carbon and all hydrogen atoms are 1:4 at high and 2:5 at low pressure, and approximately the same as in the nonequilibrium simulations. Deviations between EMD and NEMD results can only in part be ascribed to the lack of statistics. As in the case of the normal mode analysis, the partial atomic relaxation rates calculated by expression like (16), (17), and (18) cannot be exactly identified with the nonequilibrium atomic energy fluxes.

The vibrational relaxation rates were calculated summing up all partial atomic rates. This resulted in relaxation times of 389 and 19.2 ps for low and high pressure, respectively. Again, these results agree reasonably well with the NEMD rates and the values obtained by means of the normal mode analysis.

V. CONCLUSION

The results of this work clearly demonstrate that Eq. (3), representing the relaxation rate in terms of the *equilibrium* capacity TCFs, is appropriate for the description of VER of highly excited polyatomic molecules in fluids. Characterizing the solute and solvent as interacting quasiequilibrium subsystems by their own temperatures is the necessary condition (see paper I) for the applicability of Eq. (3). The nonequilibrium molecular dynamics simulations in paper II and Ref. 22 have shown that this condition is met due to fast solvent assisted intramolecular energy redistribution in azulene and efficient energy redistribution in the solvent. Additionally, in the present work it is shown that the velocity TCFs, which represent the properties of the hot solute, except for being proportional to the solute temperature, are weakly dependent on the latter and are more influenced by the solvent state. It is especially true with respect to intermode correlations that are almost completely determined by solute–solvent interactions.

The general requirement concerning the fast decay of the capacity correlations is not so easily fulfilled because the behavior of the Helfand integrands and the low frequency dependence of the Fourier transforms of the capacity TCFs show that a memory time scale can be of the order of 10 ps, which is comparable to the vibrational energy relaxation time. However, the coincidence of the relaxation times and other features of VER obtained by EMD and NEMD suggests that either these indications of long memory effects are due to the lack of statistics, or the influence of the capacity TCF tails is of minor importance.

Some differences between the relaxation rates in EMD and high temperature NEMD simulations indicate that the equilibrium and quasiequilibrium TCFs are not fully identical. More realistic azulene intramolecular and azulene– CO_2 potentials and better statistics are required to investigate the difference between these functions in more detail. Unfortunately, in spite of some information on *ab initio* potential surfaces of isolated azulene,[39] reliable data on anharmonic contributions to intramolecular potentials for such complex systems as azulene in dense environments that are suitable for MD simulations are not available at present.

ACKNOWLEDGMENTS

The authors wish to thank Professor Jürgen Troe for continued support. Financial support by the Volkswagen Stiftung (Project No. I70/627) and the Fonds der Chemischen Industrie (to C.H.) is gratefully acknowledged.

APPENDIX

Starting from Eq. (10) the velocity cross-correlation function is represented as

$$\begin{aligned}
&\langle \dot{q}_\alpha(t_1)\dot{q}_\beta(t_2)\rangle \\
&\quad = \left\langle \sum_{\gamma,\lambda} u_{\alpha\gamma}u_{\beta\lambda}\cos(\omega_\gamma t_1+\delta_{\alpha\gamma})\cos(\omega_\lambda t_2+\delta_{\beta\lambda})\right\rangle \\
&\quad \cong \langle u_{\alpha\beta}u_{\beta\beta}\{\cos[\omega_\beta(t_1+t_2)+\delta_{\alpha\beta}+\delta_{\beta\beta}] \\
&\qquad + \cos[\omega_\beta(t_2-t_1)+\delta_{\alpha\beta}-\delta_{\beta\beta}]\}\rangle \\
&\qquad + \langle u_{\alpha\alpha}u_{\beta\alpha}\{\cos[\omega_\alpha(t_1+t_2)+\delta_{\alpha\alpha}+\delta_{\beta\alpha}]+\cos[\omega_\alpha(t_2 \\
&\qquad - t_1)+\delta_{\beta\alpha}-\delta_{\alpha\alpha}]\}\rangle, \qquad \text{(A1)}
\end{aligned}$$

where angular brackets designate the ensemble average. The squares of the nondiagonal velocity amplitudes are neglected here as they are small in comparison to the terms kept in Eq. (A1). As the cross-correlation function depends only on the time internal t_2-t_1,

$$\begin{aligned}
&\langle u_{\alpha\beta}u_{\beta\beta}\cos(\delta_{\alpha\beta}+\delta_{\beta\beta})\rangle = \langle u_{\alpha\beta}u_{\beta\beta}\sin(\delta_{\alpha\beta}+\delta_{\beta\beta})\rangle = 0, \\
&\langle u_{\alpha\alpha}u_{\beta\alpha}\cos(\delta_{\alpha\alpha}+\delta_{\beta\alpha})\rangle = \langle u_{\alpha\alpha}u_{\beta\alpha}\sin(\delta_{\alpha\alpha}+\delta_{\beta\alpha})\rangle = 0. \qquad \text{(A2)}
\end{aligned}$$

This means that the sum of two random phases with equal second indices is also a random phase symmetrically distributed around horizontal and vertical directions in the

angle plane. However, to preserve the dependence on $t_2 - t_1$, the distribution of the difference of these phases cannot be so symmetric.

The static velocity cross-correlation function [Eq. (A1) at $t_2 = t_1$] is equal to zero. Calculating this function explicitly and using Eq. (A2) one concludes that

$$\langle u_{\beta\beta} u_{\alpha\beta} \cos(\delta_{\beta\beta} - \delta_{\alpha\beta}) \rangle = -\langle u_{\alpha\alpha} u_{\beta\alpha} \cos(\delta_{\alpha\alpha} - \delta_{\beta\alpha}) \rangle. \tag{A3}$$

Then Eq. (A1) is represented by

$$\begin{aligned} &\langle \dot{q}_\alpha(0) \dot{q}_\beta(t) \rangle \\ &= \langle u_{\alpha\alpha} u_{\beta\alpha} \cos(\delta_{\alpha\alpha} - \delta_{\beta\alpha}) \rangle [\cos(\omega_\alpha t) - \cos(\omega_\beta t)] \\ &\quad + \langle u_{\alpha\alpha} u_{\beta\alpha} \sin(\delta_{\beta\alpha} - \delta_{\alpha\alpha}) \rangle \sin(\omega_\alpha t) \\ &\quad + \langle u_{\alpha\beta} u_{\beta\beta} \sin(\delta_{\beta\beta} - \delta_{\alpha\beta}) \rangle \sin(\omega_\beta t). \end{aligned} \tag{A4}$$

If the random phase entering Eq. (A4) are strongly correlated so that their difference belongs mainly to the left or to the right half of the angle plane, then the time behavior of the cross-correlation function is determined by the first term of Eq. (A4). Its spectrum consists of two peaks at the mode eigenfrequencies with opposite signs. In accordance with the sum rule the integral over frequency of the Fourier transform of the cross-correlation function is equal to its static value, i.e., zero. The frequency integral over one of the peaks, say from zero to approximately half of the frequency sum $\omega_\alpha + \omega_\beta$ gives the effective magnitude of the velocity cross correlations entering Eq. (A3). These peaks are broadened due to fluctuations of frequencies and amplitudes, damping and dephasing[40] processes, which are very important here because the multipliers of the trigonometric functions in Eq. (A4) are functions of time and their properties are defined by the character of the solute–solvent clusters, their lifetime, and initial condition of cluster formation. Figure 3 shows that such a behavior is characteristic, for example, for modes 1 and 9 or 5 and 9.

In the case when fluctuating phases of two modes are weakly correlated, contributions of all terms in Eq. (A4) are approximately of the same order and due to random fluctuations of signs and values of the trigonometric functions entering the mean values the cross correlation function spectrum will consist of a sequence of random numbers of both signs near the mode frequencies like the cross-correlation spectrum for modes 1 and 11. Of course, the latter can be a result of poor statistics, too. After proper averaging the spectrum may degenerate to a smooth curve of lower amplitude.

[1] R. M. Whitnel, K. R. Wilson, and J. T. Hynes, J. Phys. Chem. **94**, 8625 (1990); J. Chem. Phys. **96**, 5354 (1992).
[2] S. A. Adelman, R. Mularidhar, and R. H. Stole, J. Chem. Phys. **95**, 2738 (1991).
[3] I. Ohmine and H. Tanaka, Chem. Rev. **93**, 2545 (1993).
[4] J. C. Owrutsky, D. Raftery, and R. M. Hochstrasser, Annu. Rev. Phys. Chem. **45**, 519 (1994).
[5] K. Lenz, M. Pfeifer, A. Lau, and T. Elsaesser, Chem. Phys. Lett. **229**, 340 (1994).
[6] J. S. Bader and B. J. Berne, J. Chem. Phys. **100**, 8359 (1994).
[7] T. Lenzer, K. Luther, J. Troe, R. G. Gilbert, and K. F. Lim, J. Chem. Phys. **103**, 626 (1995).
[8] G. Lendvay and G. C. Schatz, in *Advances in Chemical Kinetics and Dynamics*, edited by J. R. Barker (JAI, London, 1995), Vol. 2B.
[9] R. G. Gilbert, Aust. J. Chem. **48**, 1787 (1995).
[10] P. Moore, A. Tokmakoff, T. Keyes, and M. D. Fayer, J. Chem. Phys. **103**, 3325 (1995).
[11] R. Rey and J. T. Hynes, J. Chem. Phys. **104**, 2356 (1996).
[12] D. Schwarzer, J. Troe, M. Votsmeier, and M. Zerezke, J. Chem. Phys. **105**, 3121 (1996).
[13] S. A. Egorov and J. L. Skinner, J. Chem. Phys. **105**, 7047 (1996); **106**, 1034 (1997).
[14] J. Benzler, S. Linkerdörfer, and K. Luther, J. Chem. Phys. **106**, 4992 (1997).
[15] R. E. Larsen, E. F. David, G. Goodyear, and R. M. Stratt, J. Chem. Phys. **107**, 524 (1997); G. Goodyear and R. M. Stratt, *ibid.* **107**, 3098 (1997).
[16] B. M. Ladanyi and R. Parson, J. Chem. Phys. **107**, 9326 (1997); B. M. Ladanyi and R. M. Stratt, J. Phys. Chem. **102**, 1068 (1998).
[17] S. A. Egorov and B. J. Berne, J. Chem. Phys. **107**, 6050 (1997).
[18] D. Schwarzer, J. Troe, and M. Zerezke, J. Chem. Phys. **107**, 8380 (1997); J. Phys. Chem. A **102**, 4207 (1998).
[19] R. Rey and J. T. Hynes, J. Chem. Phys. **108**, 142 (1998).
[20] R. Karrlein and H. Grabert, J. Chem. Phys. **108**, 4972 (1998).
[21] C. Heidelbach, I. Fedchenia, D. Schwarzer and J. Schroeder, J. Chem. Phys. **108**, 10152 (1998).
[22] C. Heidelbach, J. Schroeder, D. Schwarzer, and V. S. Vikhrenko, Chem. Phys. Lett. **291**, 333 (1998).
[23] C. Heidelbach, Ph.D. thesis, Georg-August-Universitat, Goettingen, 1998.
[24] V. S. Vikhrenko, C. Heidelbach, D. Schwarzer, V. B. Nemtsov, and J. Schroeder, J. Chem. Phys. **110**, 5273 (1999).
[25] C. Heidelbach, V. S. Vikhrenko, D. Schwarzer, and J. Schroeder, J. Chem. Phys. **110**, 5286 (1999).
[26] J. Boon and S. Yip, *Molecular Hydrodynamics* (McGraw–Hill, New York, 1980).
[27] K. Lindenberg and B. J. West, *The Nonequilibrium Statistical Mechanics of Open and Closed Systems* (VCH, New York, 1990).
[28] D. Zubarev, V. Morozov, and G. Repke, *Statistical Mechanics of Nonequilibrium Processes* (Akademie, Berlin, 1996, 1997), Vols. 1, 2.
[29] K. F. Everitt, S. A. Egorov, and J. L. Skinner, Chem. Phys. **235**, 115 (1998); K. F. Everitt and J. L. Skinner, J. Chem. Phys. **110**, 4467 (1999).
[30] M. Vergeles and G. Szamel, J. Chem. Phys. **110**, 6827 (1999).
[31] Harvard University. CHARM 24.B1 (1995).
[32] M. P. Allen and D. J. Tildesly, *Computer Simulation of Liquids* (Oxford University Press, Oxford, 1987).
[33] W. H. Press, S. A. Teukolsky, W. T. Vetterling, and B. P. Flannery, *Numerical recipes in C. The Art of Scientific Computing*, 2nd ed. (Cambridge University Press, Cambridge, 1992).
[34] The generalized external normal forces posses nonzero mean values that result in the distortion of the isolated azulene equilibrium configuration in the solvent. These mean values were subtracted so that only fluctuating forces were taken into account in Eq. (6). However, it does not change the integrals of the capacity time correlation functions because the velocity TCFs being integrated over time yield the time derivative of the mean square displacements of normal coordinates that become equal to zero after a short initial period.
[35] Our model of the azulene–carbon dioxide system does not take into account polarization effects, which may be responsible for the described redshift of the infrared band of an in-plane vibration in solutions [see R. S. Urdahl, K. D. Rector, D. G. Myers, P. H. Davis, and M. D. Fayer, J. Chem. Phys. **105**, 8973 (1996)]. The analogous problem of the density dependence of the Raman frequency shift, which can be positive or negative depending on the molecule considered and on thermodynamic conditions, is discussed by M. E. Kooi, J. P. J. Michels, and J. A. Schouten, J. Chem. Phys. **110**, 3023 (1999).
[36] TCFs of different quantities of the same time parity are even functions of time and thus their spectra are real.
[37] E. Helfand, Phys. Rev. **119**, 1 (1960); Phys. Fluids **4**, 681 (1961).
[38] J. R. Dorfman and P. Gaspard, Phys. Rev. E **51**, 28 (1995); J. J. Erpenbeck *ibid.* **52**, 4296 (1995).
[39] F. Negri and M. Z. Zgierski, J. Chem. Phys. **99**, 4318 (1993).
[40] H. Ueba, Prog. Surf. Sci. **55**, 115 (1997).